Modeling of Poly(phenylene oxide) Reactors

M. MISRA and SANTOSH K. GUPTA*

Department of Chemical Engineering, Indian Institute of Technology, Kanpur-208016, India

SYNOPSIS

A simple model is presented for the polymerization of poly(phenylene oxide) (PPO) in the presence of mass-transfer limitations. The mass balance and moment equations for this system compose a hierarchy of infinite ordinary differential equations. Closure conditions similar to those used for nylon 6 are used to truncate the set of moment equations. The rate constants are adjusted to achieve a reasonable fit between model predictions and one set of available experimental data on the variation of the number-average chain length (μ_n) with time. The monomer conversion and the polydispersity index (PDI) are predicted. The PDI of the entire macromolecular species is found to vary with time in an interesting manner (a decrease is predicted with time during certain periods). This is due to the effect of mixing of two sets of macromolecular species present in the reaction mass having different concentrations, as well as different *individual* values of μ_n and PDI. Sensitivity results are reported to identify the important parameters and operating conditions. It is found that the values of μ_n are very sensitive to even small changes in the operating conditions which decrease the mass-transfer rates. © 1995 John Wiley & Sons, Inc.

INTRODUCTION

Poly(phenylene oxide) (PPO), commercially available as Noryl® (registered trademark of GE), is an extremely important engineering thermoplastic. It has a high glass transition temperature (205–210°C)[1] and decomposes only above about 400°C. The backbone comprises phenyl rings, because of which it has a high mechanical strength, even at −200°C.[2] In addition, this polymer has high compatibility, easy processability, and glossy looks. Because of these several advantages, PPO is carving out a niche for itself in the speciality polymer market. Its importance is reflected in the reviews[3–5] published in recent years.

High molecular weight poly(phenylene ethers) can be polymerized by the catalytic oxidation of 2,6-disubstituted phenols in solution, with oxygen gas sparged through the reactor. The first successful polymerizations were reported by Hay et al.[6,7] who used amine complexes of copper salts as the polymerization catalyst. Endres and co-workers[8,9] reported experimental results on the oxidation of 2,6-dimethylphenol in the presence of copper(I) chloride in pyridine solvent. They inferred that the reaction proceeds *primarily* by bifunctional, step-growth polymerization. Their experimental results suggested that the equal reactivity hypothesis applied. Finkbeiner et al.[10] focused attention on the role of oxygen and concluded that copper(II) was the true oxidizing agent in the oxidative coupling reaction and that the sole function of oxygen was to oxidize copper(I) to copper(II). A Michaelis–Menten-type empirical kinetic model was proposed by Tsuchida et al.[11] to describe the polymerization kinetics. Mobley[12] accounted for catalyst deactivation during polymerization and also incorporated the effect of unequal reactivity between monomer and higher oligomers in his improved kinetic model. Unfortunately, none of the early models is detailed and rigorous enough for use in the simulation, optimization, and control of industrial PPO reactors, because of their semiempirical nature.

In this study, we present a simple kinetic scheme for the polymerization of 2,6-dimethylphenol and account for the simultaneous dissolution of oxygen from the bubbles into the liquid medium and its consumption by reaction while oxidizing copper(I)

* To whom correspondence should be addressed.

Journal of Applied Polymer Science, Vol. 58, 1877–1890 (1995)
 CCC 0021-8995/95/101877-14

to copper(II). Mass balance equations have been written for the various species present in the reaction mass. They constitute an infinite set of coupled ordinary differential equations (ODEs). An established method of solving such equations is by summing them up appropriately to give an equivalent set of infinite, coupled ODEs for the moments of the chain length distribution.[13] The advantage of solving the moment equations instead of the mass balance equations is that the hierarchy of moment equations can be broken by using closure conditions, and results of interest can be obtained by integrating a much smaller set of these equations.

Closure conditions similar to those used for nylon 6 polymerization[13,14] have been found to work for PPO polymerization as well. The values of the rate constants were *tuned* using the Box complex algorithm[15] using the experimental data of Endres and Kwiatek.[8] Sensitivity studies were carried out to identify the important rate constants. In addition, step changes in some important reactor operating conditions were effected and their influence on the polymerization studied. These simulate the effects of changing the oxygen bubbling rate, temperature of the reaction mass, stirring speed, etc.

FORMULATION

Table I shows the four-step kinetic model for the polymerization of 2,6-dimethylphenol (2,6-DMP). This is a *simplified* representation of the mechanism of polymerization presented by Aycock et al.[3] The first reaction is the oxidation of Cu^+ by oxygen and its complex formation with pyridine. The activated complex reacts with the monomer to produce an ar-

Table I Detailed Reactions for PPO Polymerization

1. Catalyst Oxidation :

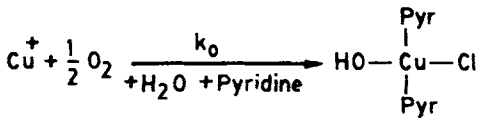

2. Aryloxy Radical Generation :

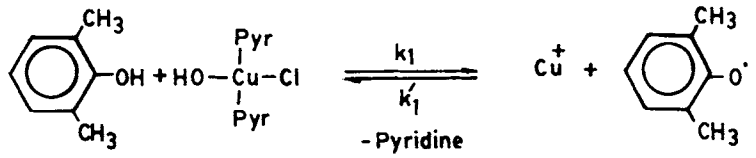

3. Polycondensation :

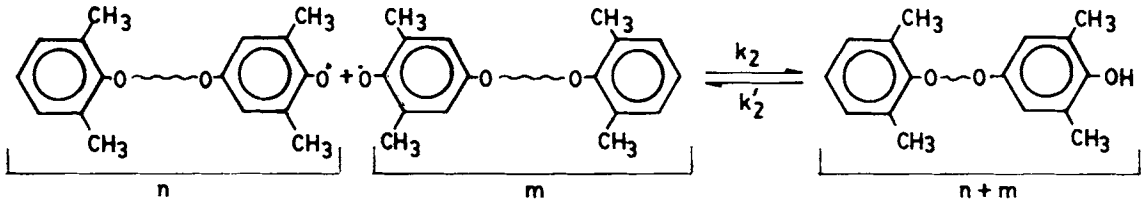

4. Polyaddition :

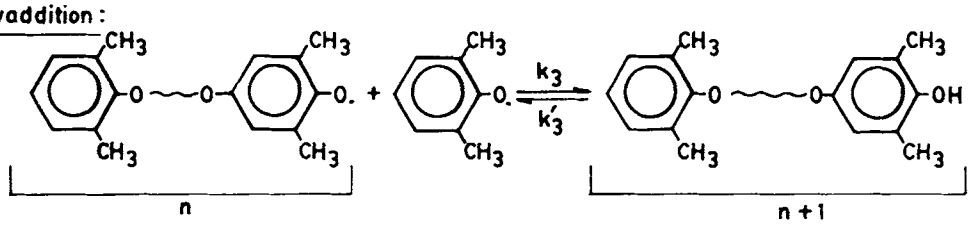

yloxy radical. These radicals can grow both by step growth as well as chain-growth mechanisms, giving long-chain PPO molecules. The actual mechanism suggested by Aycock et al.[3] is far more complex, involving intermediates like quinol ethers and quinone ketals, but Table I captures the *essential* features of PPO polymerization and has been arrived at after exploring a few more kinetic schemes (which are computationally more intensive, but do not give much better results). In addition, the experimental data reported by Endres and Kwiatek[8] on the evolution of the number-average chain length, μ_n, with time, t, for PPO shows a striking similarity with the $\mu_n(t)$ for nylon 6, and so it is felt that the basic kinetic schemes for these two systems should be somewhat similar. It may be mentioned that nylon 6 is associated with a ring-opening step leading to the formation of aminocaproic acid, which polymerizes by both the step-growth and chain-growth mechanisms, akin to what is depicted in Table I. In fact, we used the terminology "polycondensation" and "polyaddition" for reactions 3 and 4 in Table I (instead of the more rigorous terms, step growth and chain growth), following the usage of these terms for nylon 6. The kinetic scheme of Table I can be rewritten schematically as in Table II, in terms of species R_n and D_n.

Oxygen gas is sparged through the liquid reaction mixture. Oxygen dissolves in the medium, there being a mass-transfer resistance associated with this step. The dissolved oxygen oxidizes copper(I) to copper(II), as per the first equation in Tables I and II. Pure oxygen is usually sparged into the system at a pressure slightly above atmospheric. In the

Table II Kinetic Scheme for 2,6-DMP Polymerization

1. Catalyst oxidation:

$$Cu^+ + \tfrac{1}{2}\,O_2 \xrightarrow[k_0]{\text{Pyridine, } H_2O} Cu^{2+}$$

2. Aryloxy radical generation:

$$D_n + Cu^{2+} \underset{k_1'}{\overset{k_1}{\rightleftarrows}} R_n + Cu^+ \quad n = 1, 2, 3, \cdots$$

3. Polycondensation:

$$R_n + R_m \underset{k_2'}{\overset{k_2}{\rightleftarrows}} D_{n+m} \quad m = 1, 2, 3, \cdots$$

$$n = m, m + 1, m + 2, \cdots$$

(except $m = n = 1$)

4. Polyaddition:

$$R_n + R_1 \underset{k_3'}{\overset{k_3}{\rightleftarrows}} D_{n+1} \quad n = 1, 2, 3, \cdots$$

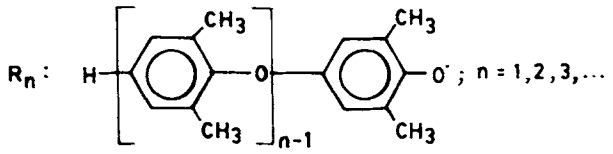

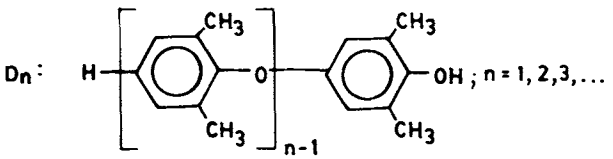

model developed herein, we neglected the pressure buildup above the liquid surface in the reactor, i.e., the system is vented (and oxygen recycled). This is often what is used industrially and is also the experimental condition used by Endres and Kwiatek.[8]

The mass balance equations for the individual molecular species for this system are given in Table III. In writing these equations, we assumed that the (bulk) liquid is well mixed and that there is no gas-film resistance to diffusion (i.e., pure O_2 is being sparged). Oxygen diffuses from the bubbles through a thin liquid film. Reaction 1 (Table I) occurs in the "bulk" of the liquid. We assume that there is no reaction inside the thin liquid film. These are reasonable approximations to make for sparged polymerization reactors, and similar approximations have been used earlier for modeling sparged polypropylene reactors.[16] The liquid-film mass-transfer coefficient at the gas (bubble)-liquid interface, k_{gl}, and the gas-liquid interfacial area per unit total volume, a_{gl}, are estimated using the correlations given in Table I of Sau and Gupta[16] which have been compiled from Refs. 17–20. The values of the physical properties of oxygen and pyridine, as well as the parameters of the (laboratory-scale) reactor (of Endres and Kwiatek,[8] for which some experimental μ_n data are available in the open literature), are given[17,20,21,†] in Table IV. The equilibrium concentration of oxygen at the gas–liquid interface, $[O_2]^*$, at the given temperature and pressure is estimated using the ideal solubility concept (Ref. 20, p. 337) with vapor pressure of oxygen estimated using the Antoine equation[20] with parameters from Ref. 20. The mole fraction of oxygen at equilibrium (at 1 atm and 300 K) is obtained as 1.156×10^{-3}. This corresponds to $[O_2]^* = 0.0188$ mol dm^{-3}. It is to be emphasized that only approximate values of $[O_2]^*$ are required, since sensitivity tests (described later) reveal that the number-average chain length, polydispersity index (PDI), and the monomer conversion are relatively insensitive to its exact value.

† An order of magnitude estimate is used.

Table III Mass Balance Equations for the Various Species

$$\frac{d[D_1]}{dt} = -k_1[Cu^{2+}][D_1] + k_1'[Cu^+][R_1] \tag{1}$$

$$\frac{d[D_2]}{dt} = -k_1[Cu^{2+}][D_2] + k_1'[Cu^+][R_2] + k_3[R_1]^2 - k_3'[D_2] \tag{2}$$

$$\frac{d[D_n]}{dt} = -k_1[Cu^{2+}][D_n] + k_1'[Cu^+][R_n] + k_3[R_1][R_{n-1}] - k_3'[D_n] + k_2 \sum_{m=1}^{n-2} [R_m][R_{n-m}] - 2(n-2)k_2'[D_n]; \quad n = 3, 4, 5, \cdots \tag{3}$$

$$\frac{d[R_1]}{dt} = -k_1[Cu^{2+}][D_1] - k_1'[Cu^+][R_1] - k_2[R_1] \sum_{m=2}^{\infty} [R_m] + 2k_2' \sum_{m=3}^{\infty} [D_m] - k_3[R_1]\left\{2[R_1] + \sum_{m=2}^{\infty} [R_m]\right\} + k_3'\left\{2[D_2] + \sum_{m=3}^{\infty} [D_m]\right\} \tag{4}$$

$$\frac{d[R_n]}{dt} = -k_1[Cu^{2+}][D_n] - k_1'[Cu^+][R_n] - k_2[R_n]\left\{[R_1] + 2\sum_{m=2}^{\infty} [R_m]\right\} + 2k_2'\left\{[D_{n+1}] + 2\sum_{m=n+2}^{\infty} [D_m]\right\} - k_3[R_1][R_n] + k_3'[D_{n+1}]; \quad n = 2, 3, 4, \cdots \tag{5}$$

$$\frac{d[Cu^+]}{dt} = -k_0[Cu^+][O_2]^{1/2} + k_1[Cu^{2+}] \sum_{n=1}^{\infty} [D_n] - k_1'[Cu^+] \sum_{n=1}^{\infty} [R_n] \tag{6}$$

$$\frac{d[Cu^{2+}]}{dt} = -\frac{d[Cu^+]}{dt} \tag{7}$$

$$\frac{d[O_2]}{dt} = k_{gl}a_{gl}([O_2]^* - [O_2]) - \frac{1}{2}k_0[Cu^+][O_2]^{1/2} \tag{8}$$

Table IV Physical Properties and Reactor Parameters[a] Used[17,20,21,b]

Reactor parameters

V_g = superficial inlet gas velocity = 0.8 (dm s^{-1})[17]
d_t = reactor diameter[b] = 1.0 dm
d_i = impeller diameter = (d_t/3) dm
V_L = total volume of liquid in the reactor = 0.785 dm^3
P = pressure = 1.013 bar
T = system temperature = 300 K

Property	Oxygen	Pyridine
Surface tension[21], σ	—	38.0 dyne dm^{-1} s^{-1}
Density,[20] ρ_g, ρ_L	From ideal gas law	983 g dm^{-3}
Viscosity,[21] μ_g, μ_L	2.018×10^{-3} g dm^{-1} s^{-1}	0.0974 g dm^{-1} s^{-1}
Critical pressure,[20] P_c	50.4 bar	—
Critical temp,[20] T_c	154.6 K	—
Diffusivity[a] of O_2 in pyridine, D_L	5.0×10^{-6} dm s^{-1}	—

[a] Notations as in Ref. 16; reactor parameters are typical of the laboratory reactor used by Endres and Kwiatek.[8]
[b] An order of magnitude is estimated.

A few differences of the kinetic scheme of Table I from that for nylon 6 need to be pointed out at this stage, since these lead to slightly different mass balance equations (Table III). The reaction

$$R_n + R_1 \rightarrow D_{n+1}; \quad n \neq 1 \tag{1}$$

is included in both the polycondensation and polyaddition steps in Table II. These are kinetically different since the polycondensation step is via a quinone–ketal intermediate,[3] while the polyaddition step is via a quinol–ether[3] intermediate. Also, a total of $2(n-2)$ possibilities (internal locations) exist for the reverse reaction for D_n, since, again, quinone–ketal intermediates are involved.

A well-established technique to solve the infinite set of mass balance equations (of Table III) is to write the corresponding moment equations. Equations for the zeroth, first, and second moments of the polymeric species, as defined by

$$\mu_k \equiv \sum_{n=1}^{\infty} n^k [D_n] \tag{a}$$

$$\lambda_k \equiv \sum_{n=1}^{\infty} n^k [R_n] \tag{b} (2)$$

are given in Table V along with some additional ODEs to make the set complete. A moment closure equation relating μ_3 to μ_0, μ_1 and μ_2, as well as a closure condition for $[D_2]$ are required before we can integrate these equations. Since the kinetic scheme for PPO polymerization is somewhat similar to that of nylon 6, closure conditions identical in form[14] to those used for nylon 6 have been used in this work as well. The results obtained were found to be in excellent agreement with the experimental data of Endres and Kwiatek.[8] The theoretical predictions of $\mu_n(t)$ were also found to be relatively insensitive to slight changes in the closure equations. These tests suggest that the closure equations used are appropriate. The *complete* set of equations is given in Table V. The equation for $d[R_1]/dt$ in Table V includes a term $\mu_0 - [D_1] - [D_2]$. This term could take on negative values near $t = 0$, due to the closure approximation, $[D_2] = \alpha_1[D_1]$, used. To avoid this, a multiplying factor, α_{mul}, is used with this term, which is zero for negative values of $\mu_0 - [D_1] - [D_2]$ and unity otherwise. This prevents unreasonable results from being generated at $t \sim 0$.

The rate constants used for obtaining the μ_n, conversion, and PDI histories were *tuned* using the Box[15] complex algorithm. Initial guesses for some of these constants were obtained from the literature,[22] while for the remaining, starting estimates were obtained by trial and error.[23] The objective function used to obtain the "best-fit" value of the rate constants was taken as

$$\text{Min } E \equiv \sum_{i=1}^{N} w_i \left| (\mu_{n,i}^{\text{expt}} - \mu_{n,i}^{\text{theor}}) \right| / \mu_{n,i}^{\text{expt}} \tag{3}$$

In this equation, $\mu_{n,i}^{\text{expt}}$ are the experimental values of μ_n of Endres and Kwiatek,[8] while $\mu_{n,i}^{\text{theor}}$ are values

Table V Complete Set of Equations for PPO Polymerization

Moment equations:

$$\frac{d\mu_0}{dt} = -k_1[Cu^{2+}]\mu_0 + k_1'[Cu^+]\,\lambda_0 + k_2\lambda_0(\lambda_0 - [R_1]) - 2k_2'(\mu_1 - 2\mu_0 + [D_1]) + k_3[R_1]\lambda_0 - k_3'(\mu_0 - [D_1]) \quad (1)$$

$$\frac{d\mu_1}{dt} = -k_1[Cu^{2+}]\mu_1 + k_1'[Cu^+]\lambda_1 + k_2\{2\lambda_0\lambda_1 - [R_1](\lambda_0 + \lambda_1)\} - 2k_2'(\mu_2 - 2\mu_1 + [D_1]) + k_3[R_1](\lambda_0 + \lambda_1) - k_3'(\mu_1 - [D_1]) \quad (2)$$

$$\frac{d\mu_2}{dt} = -k_1[Cu^{2+}]\mu_2 + k_1'[Cu^+]\lambda_2 + k_2\{2(\lambda_0\lambda_2 + \lambda_1^2) - [R_1](\lambda_0 + 2\lambda_1 + \lambda_2)\} - 2k_2'(\mu_3 - 2\mu_2 + [D_1]) + k_3[R_1](\lambda_2 + 2\lambda_1 + \lambda_0) - k_3'(\mu_2 - [D_1]) \quad (3)$$

$$\frac{d\lambda_0}{dt} = k_1[Cu^{2+}]\mu_0 - k_1'[Cu^+]\lambda_0 - 2k_2\lambda_0(\lambda_0 - [R_1]) + 4k_2'(\mu_1 - 2\mu_0 + 2[D_1]) - 2k_3[R_1]\lambda_0 + 2k_3'(\mu_0 - [D_1]) \quad (4)$$

$$\frac{d\lambda_1}{dt} = k_1[Cu^{2+}]\mu_1 - k_1'[Cu^+]\,\lambda_1 - k_2\{2\lambda_0\lambda_1 - [R_1](\lambda_0 + \lambda_1)\} + 2k_2'(\mu_2 - 2\mu_1 + [D_1]) - k_3[R_1](\lambda_0 + \lambda_1) + k_3'(\mu_1 - [D_1]) \quad (5)$$

$$\frac{d\lambda_2}{dt} = k_1[Cu^{2+}]\mu_2 - k_1'[Cu^+]\lambda_2 + k_2\{2\lambda_0\lambda_2 - [R_1](\lambda_2 + \lambda_0)\} + 2k_2'\left\{\frac{2}{3}\mu_3 - 2\mu_2 + \frac{7}{3}\mu_1 - 2\mu_0 + [D_1]\right\} - k_3[R_1](\lambda_0 + \lambda_2) + k_3'(\mu_2 - 2\mu_1 + 2\mu_0 - [D_1]) \quad (6)$$

Additional equations:

$$\frac{d[D_1]}{dt} = -k_1[Cu^{2+}][D_1] + k_1'[Cu^+][R_1] \quad (7)$$

$$\frac{d[R_1]}{dt} = k_1[Cu^{2+}][D_1] - k_1'[Cu^+][R_1] - k_2[R_1](\lambda_0 - [R_1]) + 2k_2'(\mu_0 - [D_1] - [D_2]) \times \alpha_{mul} - k_3[R_1](\lambda_0 + [R_1]) + k_3'(\mu_0 - [D_1] + [D_2]) \quad (8)$$

$$\frac{d[Cu^{2+}]}{dt} = -k_0[Cu^+][O_2]^{1/2} + k_1[Cu^{2+}]\mu_0 - k_1'[Cu^+]\lambda_0 \quad (9)$$

$$\frac{d[Cu^{2+}]}{dt} = -\frac{d[Cu^+]}{dt} \quad (10)$$

$$\frac{d[O_2]}{dt} = k_{gl}a_{gl}\{[O_2]^* - [O_2]\} - \frac{1}{2}k_0[Cu^+][O_2]^{1/2} \quad (11)$$

Closure conditions:

$$\mu_3 = \frac{\mu_2(2\mu_2\mu_0 - \mu_1^2)}{\mu_1\mu_0} \quad (12)$$

$$[D_2] = \alpha_1[D_1];\ (\alpha_1 = 0.1) \quad (13)$$

(at the same value of t) predicted by our model for any assumed set of rate constants. There are N (=6) data points available[8] in the open literature. The values of the weighting factors, w_1 to w_5, are taken as unity, while w_6 is taken as 3.0. This is to ensure the importance of the last data point (high value of μ_n). The value of E is the sum of the squares of the deviations between experimental and theoretical values of μ_n at different values of t. Minimization of E, thus, improves the agreement between theory and experiment. It may be added that there is very little experimental data reported on PPO polymerization in the open literature, and *full* confirmation of our present model has to wait until more

data (under different operating conditions) becomes available.

The number-average chain length, μ_n, has been defined in the present work as

$$\mu_n = \{(\mu_1 - [D_1]) + (\lambda_1 - [R_1])\}/\{(\mu_0 - [D_1]) + (\lambda_0 - [R_1])\} \quad (4)$$

The need for this definition of μ_n arose because when we used the conventional definition of μ_n (without subtracting $[D_1]$ and $[R_1]$ in eq. (4)), our model did not give very good agreement with the experimental data of Endres and Kwiatek[8] in the initial stages of polymerization, irrespective of the choice of the rate constants. Closer scrutiny of the experimental procedure of Endres and Kwiatek revealed that the monomeric species (and possibly some of the other lower oligomers) was dissolved out of the polymer before making dilute solutions of the latter for measuring μ_n using intrinsic viscosity. Thus, to reflect the actual compositions of the polymeric samples, species D_1 and R_1 should be excluded from the various moments, as given in eq. (4).

RESULTS AND DISCUSSION

The D02EBF subroutine of the NAG library, which uses Gear's algorithm[24] to solve stiff ODEs, was used to solve the set of equations of Table V with the starting set of values of the rate constants as given in Table VI (Set A). The initial conditions for the ODEs correspond to the experimental conditions used by Endres and Kwiatek[8]:

At $t = 0$:

$$\mu_k = 0.75 \text{ mol dm}^{-3}; \quad k = 0, 1, 2$$

$$\lambda_k = 0 \text{ mol dm}^{-3}; \quad k = 0, 1, 2$$

$$[D_1] = 0 \text{ mol dm}^{-3}$$

$$[R_1] = 0 \text{ mol dm}^{-3}$$

$$[D_2] = 0 \text{ mol dm}^{-3}$$

$$[Cu^+] = 0.045 \text{ mol dm}^{-3}$$

$$[Cu^{++}] = 0 \text{ mol dm}^{-3}$$

$$[O_2] = 0 \text{ mol dm}^{-3} \quad (5)$$

The (constant) values for k_{gl}, a_{gl}, and $[O_2]^*$ used are

$$k_{gl} = 0.030073 \text{ dm s}^{-1}$$

$$a_{gl} = 92.661 \text{ dm}^2 \text{ dm}^{-3}$$

$$[O_2]^* = 0.0188 \text{ mol dm}^{-3} \quad (6)$$

These correspond to the operating conditions used by Endres and Kwiatek.[8] Several checks were made on the computer program to ensure that it was free of errors. Also, a change in the value of the computational parameter, TOL, in the D02EBF code, from 10^{-2} to 10^{-6}, gave the same values for μ_n (up to four decimal places). A value of 10^{-4} for this parameter was used for all runs subsequently. A typical computer run took 45 s on a mainframe supermini HP 9000/850S. The results were not affected much when the closure constant, α_1, was varied from 1.0 to 0.01 or when a multiplying factor of 1.5 or 0.5 was used on the right-hand side of the closure equation for μ_3. Values of $\alpha_1 = 0.1$ and a multiplying factor of unity on the right-hand side of the closure equation for μ_3 were used for all runs hereafter. The Box complex algorithm converged to values given as Set B in Table VI. It is clear that the starting values used were very good estimates and, in fact, had been obtained earlier[23] using a slightly different kinetic scheme.

Table VI Best-fit Values of the Rate Constants for PPO Polymerization (at 300 K)

Rate Constant	Starting (A)	Best-fit (B)
k_0, dm^3 mol^{-1} s^{-1}	48.0	49.0
k_1, dm^3 mol^{-1} s^{-1}	0.571	0.568
k_2, dm^3 mol^{-1} s^{-1}	9.2528×10^2	10.749×10^2
k_3, dm^3 mol^{-1} s^{-1}	4.977×10^{-4}	4.855×10^{-4}
k'_1, dm^3 mol^{-1} s^{-1}	1.93×10^{-3}	1.781×10^{-3}
k'_2, s^{-1}	3.995×10^{-7}	4.065×10^{-7}
k'_3, s^{-1}	3.995×10^{-7}	4.448×10^{-7}

Figures 1–3 show the variations of μ_n, PDI, and monomer conversion, respectively, with time, as obtained using the best-fit values of the rate constants. Excellent agreement between experimental data[8] on μ_n and model predictions are observed. It is found that μ_n increases very slowly to about 12.5 at $t = 617$ s and then rises very sharply to about 200 at $t = 840$ s. The initial slow increase followed by a sharp rise in μ_n with time is a characteristic of both PPO and nylon 6 polymerizations and is associated with the presence of *both* step-growth and chain-growth reactions in their kinetic schemes. The fact that our model predicts the general trends of $\mu_n(t)$ confirms that we have indeed been able to identify a fairly accurate kinetic scheme for PPO.

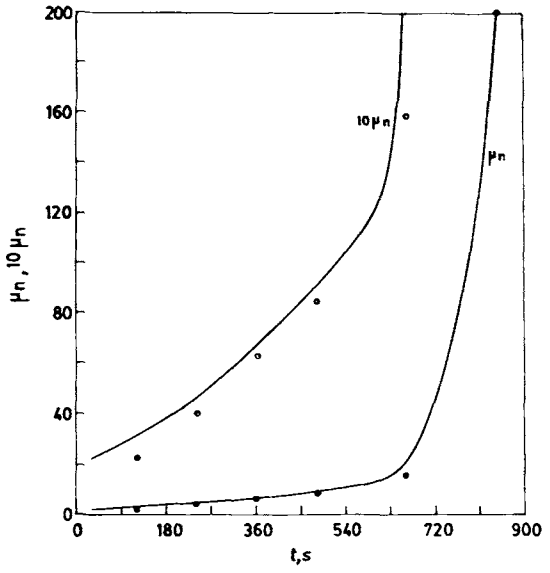

Figure 1 Variation of μ_n (and 10 μ_n for small values of t) with time using the best-fit values of the rate constants (Table VI) and conditions given in Eqs. (5) and (6). Experimental data of Endres and Kwiatek[8] also shown.

Figure 2 shows the PDI history. The PDI exhibits a local maximum at about $t \simeq 450$ s. It would be interesting to see if such a maximum is also observed experimentally, but since no data on the PDI has been reported yet, this remains purely a theoretical prediction. This unusual behavior of the PDI is primarily because the reaction mass is a mixture of two different species, R_n and D_n. The relative concentrations of these species and the *individual* values of μ_n (of the R_n and D_n species) vary with time in an interesting manner[23] to give the maximum in the PDI.

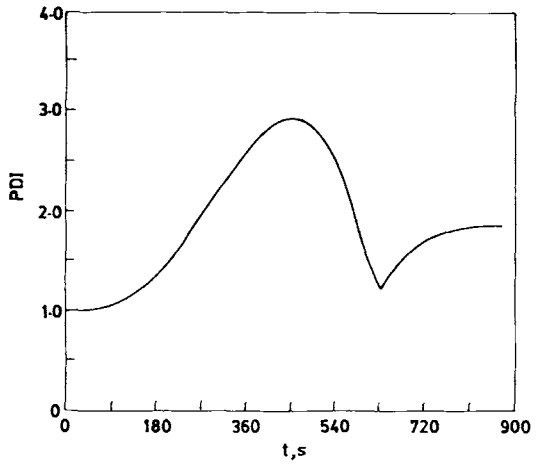

Figure 2 Variation of PDI for the same conditions as in Figure 1.

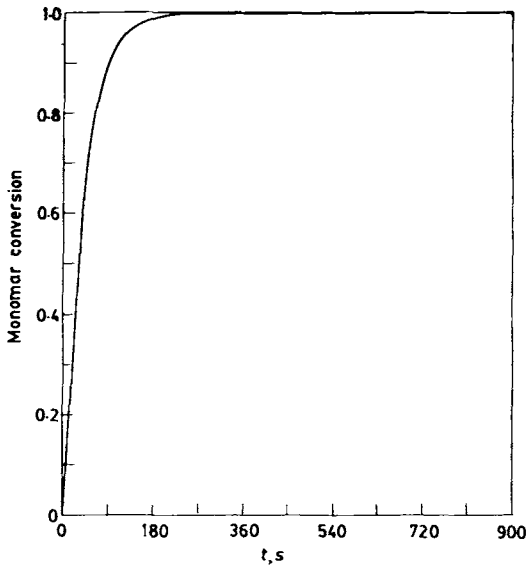

Figure 3 Variation of monomer conversion for the same conditions as in Figure 1.

Figure 3 shows the variation of the monomer conversion with time. The monomer, D_1, gets consumed very rapidly and is almost depleted by t = 180 s. Figure 4 shows the variation of the dissolved oxygen concentration in the liquid (bulk value), $[O_2]$, with time. For the given conditions, the equilibrium concentration of oxygen in pyridine (the value at the bubble-liquid interface), $[O_2]^*$, used is 0.0188 mol dm^{-3}, as discussed earlier. As seen from Figure 4, $[O_2]$ reaches close to its saturation

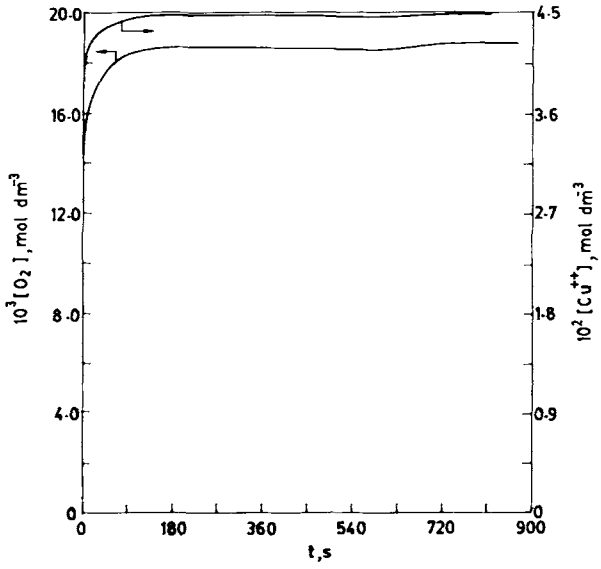

Figure 4 Variation of dissolved oxygen concentration (in the liquid bulk) and Cu^{2+} ion concentration in the liquid. Conditions same as in Figure 1.

Table VII Experimental and Theoretical Values of μ_n Under Different Conditions

t (s)	μ_n^{expt} (Ref. 8)	μ_n^{theor} (best-fit k's)	μ_n ($k_2 = 0$)	μ_n ($k_3 = 0$)	μ_n ($k_1' = k_2' = k_3' = 0$)
120	2.29	3.0886	2.006	3.031	3.0906
240	4.12	4.68121	2.022	5.031	4.6818
360	6.33	6.7104	2.040	8.127	6.7108
480	8.49	9.2190	2.058	11.193	9.2195
660	15.9	21.3281	2.084	15.772	21.3159
840	200	200.8020	2.109	20.365	200.690

value very rapidly (in about 140 s) and remains at this value throughout. A very shallow minimum is observed at about 585 s. It is interesting to see that at about this value of t the $\mu_n(t)$ curve starts rising. This is consistent with our kinetic scheme (Table II). The generation of significant amounts of high chain length D_n species around this time leads to a rapid transformation of Cu^{2+} into Cu^+ in the reaction mass (by reaction 2 in Table II). Dissolved oxygen then is rapidly consumed (by reaction No. 1), and if mass transfer does not take place at a fast enough rate, there will be a slight lowering of $[O_2]$. The variation of Cu(II) in solution, $[Cu^{2+}]$, with time is also shown in Figure 4. $[Cu^{2+}]$ rises very rapidly to about 0.044 mol dm^{-3} in about 50 s and remains at this value throughout (the maximum value of $[Cu^{2+}]$ is 0.045 mol dm^{-3}). Like $[O_2]$, $[Cu^{2+}]$ also shows a shallow local minimum at about 585 s, for the same reasons.

An interesting theoretical experiment is now conducted. We made $k_2 = 0$ (i.e., the polycondensation step is omitted) and $k_3 = 0$ (i.e., the polyaddition step is omitted) separately to see how $\mu_n(t)$ changed. Table VII shows that if $k_2 = 0$, μ_n remains low throughout (approximately 2.0). On the other hand, if k_3 is made equal to 0, μ_n increases to only about 20 (at $t \simeq 840$ s). Thus, we infer that both polyaddition and polycondensation reactions are required to yield high values of μ_n. In fact, there seems to be a synergistic effect present. A close study of Table VII indicates that the early (slow) increase in μ_n can easily be associated with the polycondensation reaction, whereas *both* the polycondensation and polyaddition reactions are necessary to explain the sharp rise in μ_n at later times.

We now carried out a detailed sensitivity study to see which of the forward rate constants from among k_0, k_1, k_2, and k_3 need to be estimated accurately. Such a study can also help in the intelligent design of experimental work in the future. We varied the rate constants by ±20%, one at a time, keeping the others at their best-fit values. Figures 5–7 show the effect of varying k_1. Significant changes are observed in the μ_n values corresponding to high values of t. The final value (at $t = 840$ s) of μ_n increases to about 840 (from 200) for a 20% increase in k_1 and decreases to about 48 for a 20% decrease in k_1. The high sensitivity of μ_n to k_1 also indicates that one must have a good temperature control of the reactor if the activation energy for this reaction is not negligible. We see from Figure 6 that although the final value of PDI has not changed much the local maximum is reached at an earlier value of t for a 20% increase in k_1. It would be interesting to confirm the existence of the PDI peak experimentally and explore whether the peak location can be used to curve-fit the values of the rate constants. Figure 7 shows faster conversion of the monomer when k_1 is increased, as expected. Values of $[O_2]$ and $[Cu^{++}]$ were found to be relatively insensitive to variations in k_1,

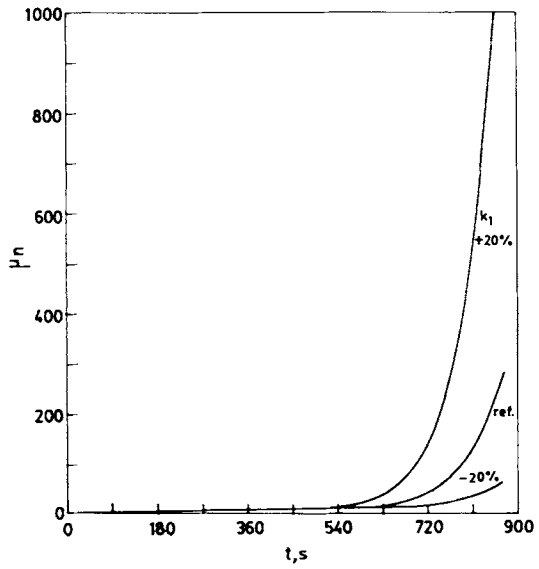

Figure 5 Effect of varying k_1 on μ_n history. Reference curve is same as in Figure 1. All other parameters except k_1 are as for Figure 1.

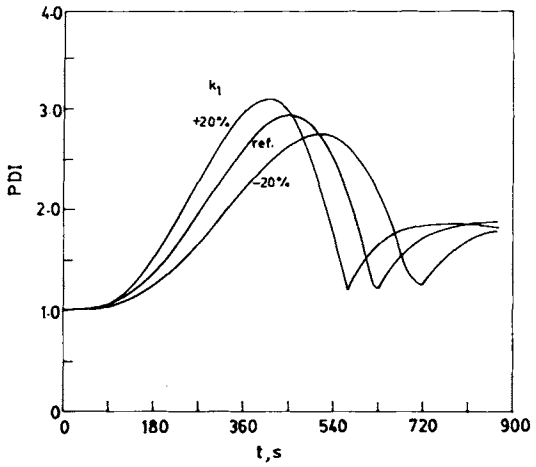

Figure 6 Effect of varying k_1 on PDI history. Other conditions same as in Figure 5.

primarily since their values are quite close to their maximum values.

Figures 8 and 9 show the results of the sensitivity test of k_3. Here, again, a 20% increase in k_3 leads to the final value (at t = 840 s) of μ_n increasing significantly from 200 to about 340. A 20% decrease in k_3 is associated with a fall of μ_n to about 97. In contrast, μ_n values are essentially unchanged for a ±20% change in k_2. This leads to the interesting observation that in the later stages of reaction ($t > 617$ s) the values of μ_n are sensitive only to the polyaddition reaction, even though the presence of the polycondensation reaction is necessary for the attainment of high values of μ_n.

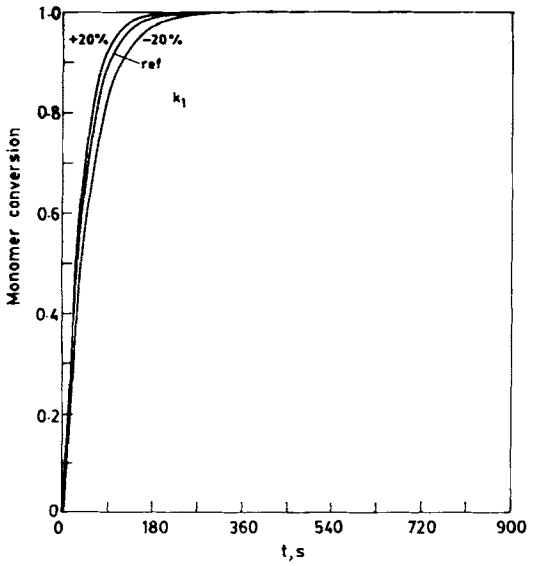

Figure 7 Effect of varying k_1 on monomer conversion history. Other conditions same as in Figure 5.

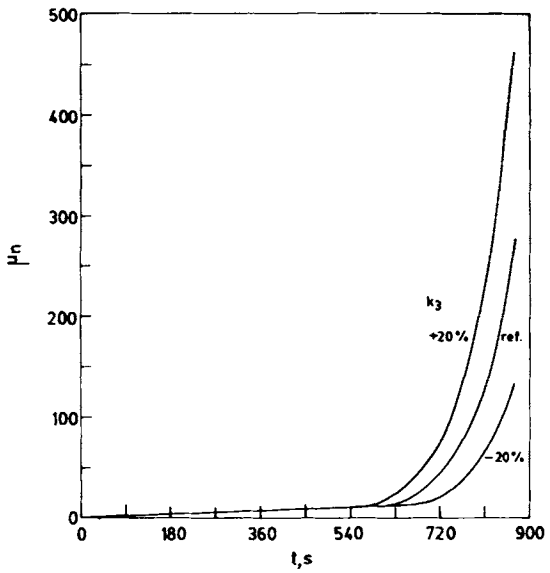

Figure 8 Effect of varying k_3 on μ_n history. Reference curve is same as in Figure 1. All other parameters except k_3 are as for Figure 1.

The effect of varying k_3 on the PDI history is shown in Figure 9. The trends are opposite to those observed on changing k_1 (Fig. 6). A 20% decrease in k_3 gives a higher peak. This is because lower values of k_3 prolong the presence of R_1 in the reaction mass, while higher-length D_n species are formed. This leads to higher polydispersities in the macromolecular mixture. The values of monomer conversion, $[O_2]$ and $[Cu^{2+}]$ were found to be relatively unaffected by variations in k_3.

Sensitivity tests performed on k_0 and k_2 revealed insignificant changes in the μ_n, PDI, monomer conversion, $[O_2]$, and $[Cu^{2+}]$ histories. Thus, we need

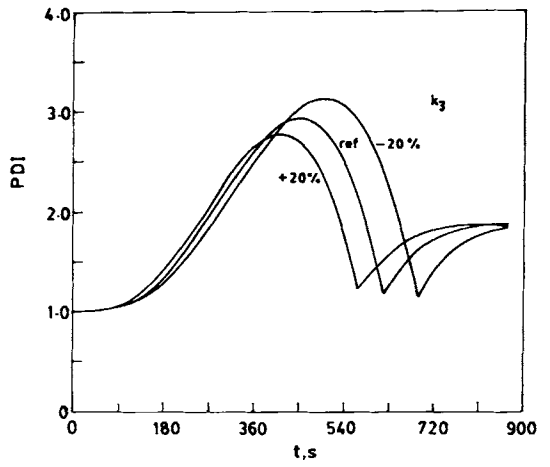

Figure 9 Effect of varying k_3 on PDI history. Other conditions same as in Figure 8.

to estimate k_1 and k_3 very accurately when more experimental results become available. It may be added that the effect of increasing temperatures can be *qualitatively* inferred from the combined effects of increasing the two sensitive rate constants, k_1 and k_3.

Since the reverse rate constants appeared to be quite low, we carried out one integration assuming $k_1' = k_2' = k_3' = 0$, for the conditions given in eqs. (5) and (6). Table VII shows that almost identical results are obtained for μ_n for the irreversible case, as for reversible polymerization. In fact, we can easily simplify the kinetic schemes and the mass balance and moment equations given in Tables II, III, and V, by dropping the terms for the reverse reactions. It is expected, however, that reversibility will play an important role at still higher values of μ_n, when the $\mu_n(t)$ curve starts flattening out, but since experimental data are not available beyond $t = 840$ s, we cannot say much about the reverse rate constants. In fact, since the role of the reverse rate constants is negligible, we are *really* curve fitting only four parameters, k_0, k_1, k_2, and k_3, in this work.

The role of some important reactor operating conditions is now studied, using the best-fit values of the rate constants. The first such condition studied is the initial monomer concentration, $[D_1]_0$ (this changes the initial values of all the μ_k also). We found that a 20% increase in $[D_1]_0$ leads to the final value (at $t = 840$ s) of μ_n increasing from 200 to 342, while a 20% decrease in $[D_1]_0$ brings μ_n at 840 s down to 96 (see Fig. 10). The PDI history also

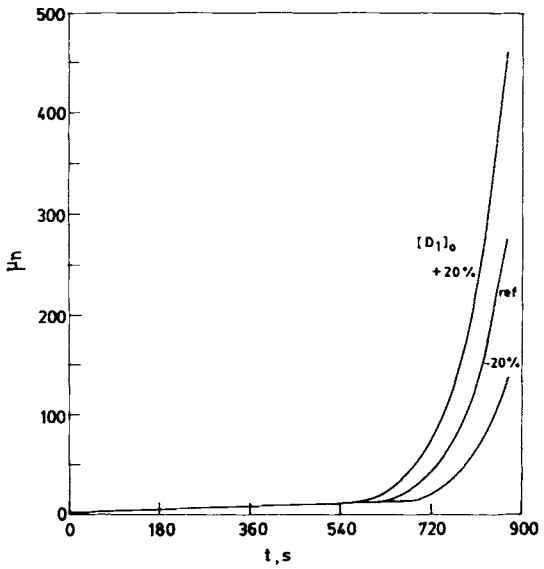

Figure 10 Effect of varying the initial monomer concentration, $[D_1]_0$, on the μ_n history. Other conditions same as in Figure 3.

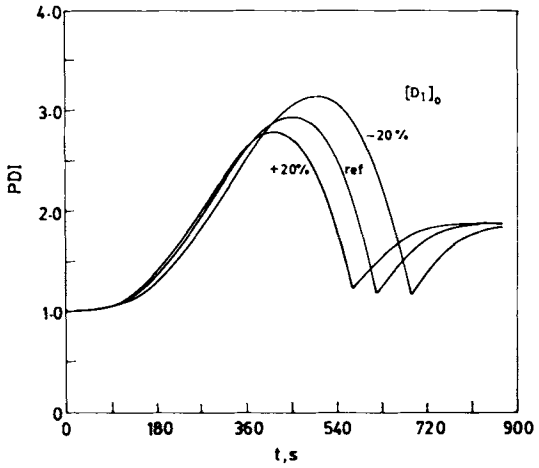

Figure 11 Effect of varying the initial monomer concentration, $[D_1]_0$, on the PDI history. Other conditions same as in Figure 3.

changes as $[D_1]_0$ is made to vary by ±20%, as shown in Figure 11. It is interesting to note that the effect of varying $[D_1]_0$ by this amount is similar to the effect of varying k_3 by ±20% (see Figs. 8 and 9). There are no discernible differences in the plots for monomer conversion, $[Cu^{2+}]$, etc., for the three values of $[D_1]_0$ studied.

The other important reactor operating variable studied is the rate of mass transfer. Since the two parameters characterizing this, k_{gl} and a_{gl}, occur as a product, only the latter ($k_{gl}a_{gl}$) is varied, and its effect on the polymerization studied in detail. We do not focus attention on the variation of the *individual physical* variables like the superficial inlet gas velocity, volumetric feed rate of gas, height and total volume of the liquid in the reactor, impeller specifications (impeller diameter, rate of rotation), etc., since their effects on $k_{gl}a_{gl}$ can easily be deduced from the correlations given by Sau and Gupta.[16] Figures 12–16 show how the μ_n, PDI, monomer conversion, $[O_2]$, and $[Cu^{2+}]$ histories change when $k_{gl}a_{gl}$ is decreased by factors of 5, 10, 20, 30, 40, and 50. It is observed that mass-transfer limitations could be quite significant, and a polymer having much lower values of μ_n would be obtained if oxygen cannot dissolve in the solvent rapidly enough. Figure 15 shows how increases in the mass-transfer rates lead to the minima in the dissolved oxygen concentration (at $t \simeq 650$ s), becoming less accentuated, as alluded to earlier. An increase in the value of $k_{gl}a_{gl}$ beyond the reference value given by eq. (6) (by factors of 5, 10, and even 100) does not lead to any significant changes in the results. This reflects the fact that the reference values used [eq. (6)] for k_{gl} and a_{gl} are such that mass-transfer resistances are not very signifi-

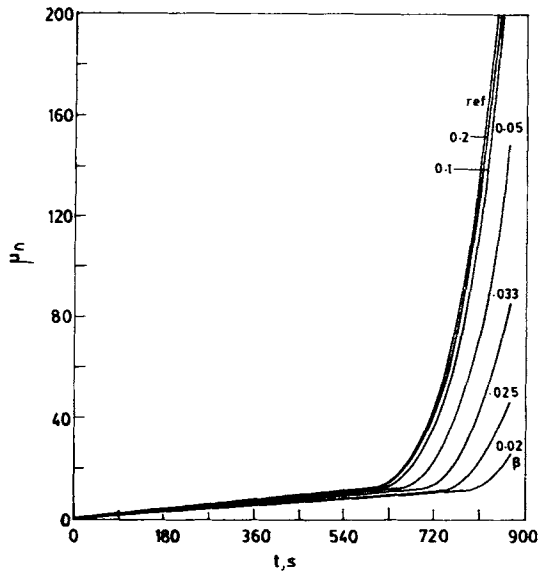

Figure 12 Effect of varying ($k_{gl}a_{gl}$) on the μ_n history. Reference curve same as in Figure 1. Values of factor, β, with $k_{gl}a_{gl} = \beta(k_{gl}a_{gl})_{ref}$, indicated.

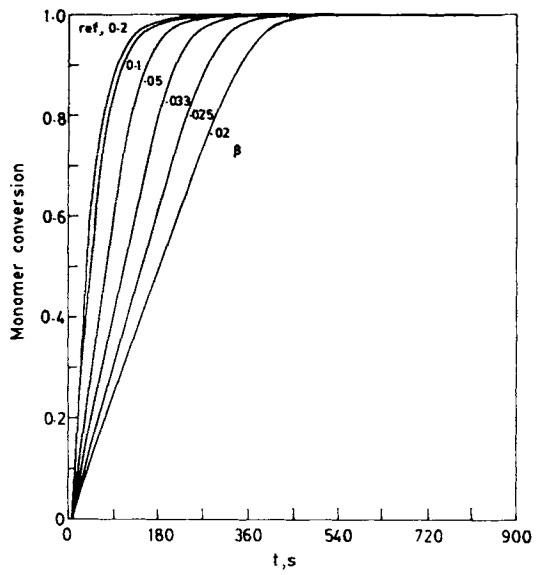

Figure 14 Effect of varying ($k_{gl}a_{gl}$) on the monomer conversion. Values of factor, β, indicated.

cant in the laboratory-scale reactor used by Endres and Kwiatek,[8] as would be expected. In fact, we modified our balance equations to remove all mass-transfer resistances, i.e., without including the first step of Table II. The modified equations were slightly different from those given in Table V. Equations (9), (10), and (11) of Table V were deleted and, instead, the following were used:

$$[Cu^+] = 0 \text{ mol dm}^{-3}$$
$$[Cu^{2+}] = 0.045 \text{ mol dm}^{-3} \quad (7)$$

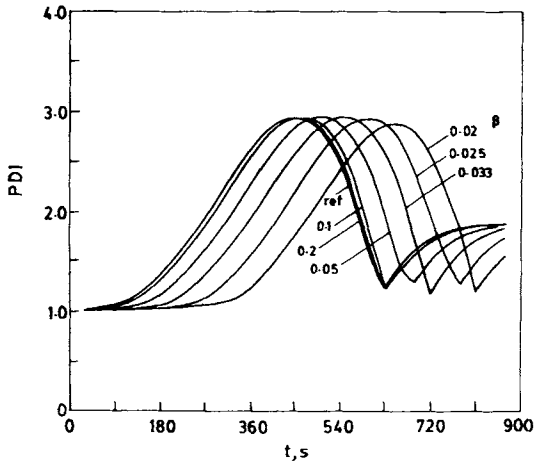

Figure 13 Effect of varying ($k_{gl}a_{gl}$) on the PDI history. Values of β (see Fig. 12) indicated.

The results obtained were very close to those obtained in the presence of mass-transfer terms [eq. (6)]. This confirms that mass-transfer resistances are negligible under the conditions used by Endres and Kwiatek.[8] However, these effects would play an important role in larger, industrial-scale reactors.

An interesting study was also carried out in which the reference value [eq. (6)] of $k_{gl}a_{gl}$ was used for $0 \leq t \leq t_1$, and, thereafter, a step change was made in the value of this product. For $t > t_1$, $k_{gl}a_{gl}$ was taken

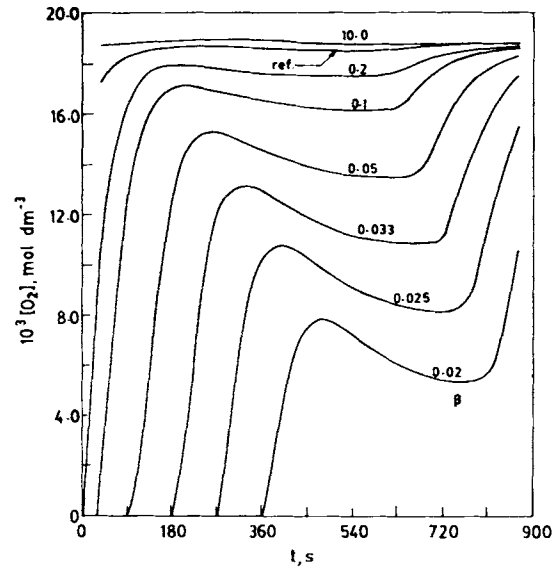

Figure 15 Effect of varying $k_{gl}a_{gl}$ on the dissolved oxygen concentration.

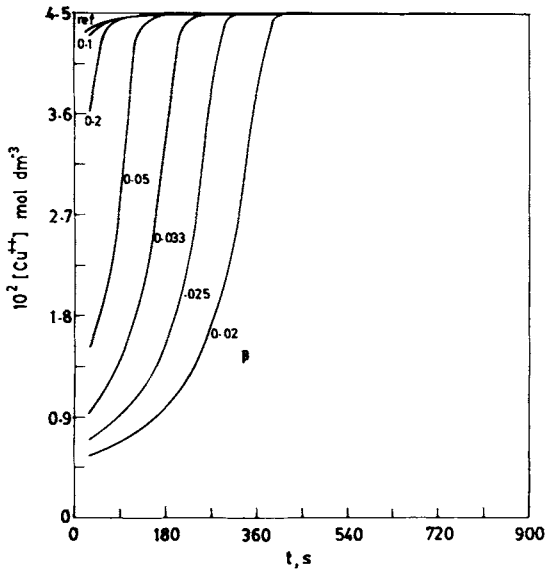

Figure 16 Effect of varying $k_{gl}a_{gl}$ on the Cu^{2+} ion concentration.

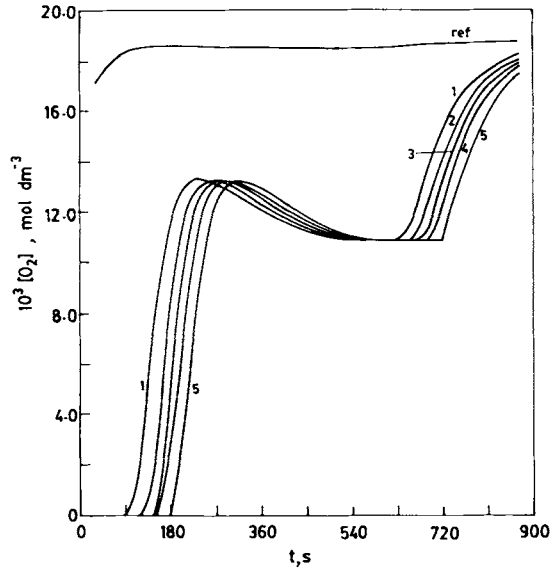

Figure 18 Effect of step decrease of $k_{gl}a_{gl}$ at $t = t_1$ on the dissolved oxygen concentration. Other conditions same as in Figure 17.

as 0.033 $(k_{gl}a_{gl})_{eq.\ (6)}$. It was found that the value of the computational parameter, TOL (in the D02EBF code), had to be reduced to 10^{-7} to obtain good results for the step tests. Figure 17 shows how μ_n varies with time for this step-test, with different values of t_1 of 0.001, 1.5, 5.0, 10.0, and 20.0 s. Figure 18 shows the dissolved oxygen concentration for these cases. Reduction of the mass-transfer rates of oxygen leads to a lowering of the values of μ_n, this change being more significant when the value of $k_{gl}a_{gl}$ is reduced early. What is to be noted from Figure 17 is the extreme sensitivity of the results to the value of t_1—lowering the mass-transfer rate a few seconds earlier, say at 5 s after the start of polymerization instead of at 10 s, could lower the final value of μ_n from about 160 to 130. Practically speaking, this implies that changes of operating conditions which lead to a reduction of the mass-transfer rate (e.g., agitator speed or rate of sparging of oxygen) even for short periods of time could have important effects on the value of μ_n. We have knowledge of some experimental evidence of such effects, but are unable to give details due to reasons of confidentiality. The fact that our simple model can mirror such behavior gives further confidence that it describes the physical situation well. The PDI shows delayed peaks as t_1 decreases, somewhat akin to that observed in Figure 13.

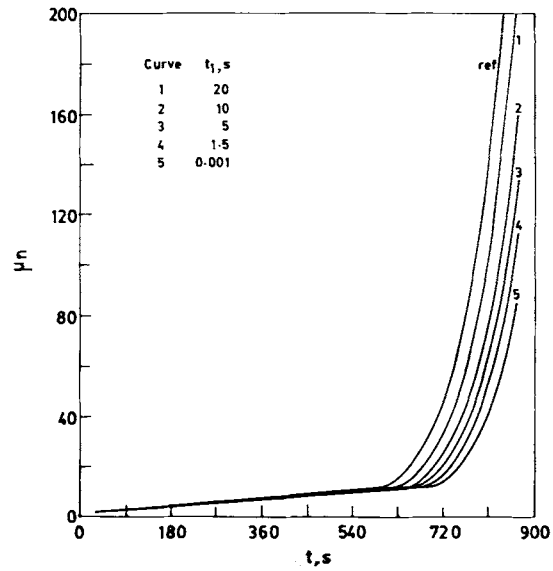

Figure 17 Effect of step-decrease of $k_{gl}a_{gl}$ at $t = t_1$ on the μ_n history. For $t \leq t_1$, reference value of $k_{gl}a_{gl}$ was used, while for $t \geq t_1$, 0.033 $(k_{gl}a_{gl})_{ref}$ was used.

CONCLUSIONS

A simple model accounting for mass transfer in the presence of polymerization reactions has been developed for PPO polymerization. The tuned model explains some scarce experimental data on μ_n history quite well. Sensitivity tests are carried out to identify the important parameters characterizing polymerization. It is found that the effect of step changes in the mass-transfer rates are quite significant.

NOMENCLATURE

a_{gl}	gas–liquid interfacial area per unit volume ($dm^2\ dm^{-3}$)
D_n	a polymer molecule (nonradical) with n repeat units
k_{gl}	liquid–film mass-transfer coefficient ($dm\ s^{-1}$)
k_i	rate constants for forward reactions ($dm^3\ mol^{-1}\ s^{-1}$ or s^{-1})
k_i'	rate constants for reverse reactions ($dm^3\ mol^{-1}\ s^{-1}$ or s^{-1})
$[O_2]$	dissolved oxygen concentration in the liquid "bulk" ($mol\ dm^{-3}$)
$[O_2]^*$	equilibrium value of the dissolved oxygen concentration at the gas–liquid interface ($mol\ dm^{-3}$)
PDI	polydispersity index of the entire macromolecular species [$\equiv (\mu_0 - [D_1] + \lambda_0 - [R_1])(\mu_2 - [D_1] + \lambda_2 - [R_1])/(\mu_1 - [D_1] + \lambda_1 - [R_1])^2$]
R_n	a polymeric aryloxy radical with n repeat units
t	time (s)

Greek Letters

λ_k	kth moment of R species; $k = 0, 1, 2$ ($mol\ dm^{-3}$) [eq. (1)]
μ_k	kth moment of D species; $k = 0, 1, 2$ ($mol\ dm^{-3}$) [eq. (1)]
μ_n	number-average chain length of the entire macromolecular species [$\equiv(\mu_1 - [D_1] + \lambda_1 - [R_1])/(\mu_0 - [D_1] + \lambda_0 - [R_1])$]
μ_w	weight-average chain length of the entire macromolecular species [$\equiv (\mu_2 - [D_1] + \lambda_2 - [R_1])/(\mu_1 - [D_1] + \lambda_1 - [R_1])$]

Symbols

[ ]	molar concentration ($mol\ dm^{-3}$)

Subscripts

0	initial value (unless otherwise specified)

REFERENCES

1. F. E. Karasz and J. M. O'Reilly, *J. Polym. Sci. Polym. Lett. Ed.*, **3,** 561 (1965).
2. J. Heijboer, *J. Polym. Sci. C,* **16,** 3755 (1968).
3. D. Aycock, V. Abolins, and D. M. White, in *Encyclopedia of Polymer Science and Engineering,* 2nd ed., H. F. Mark, N. M. Bikales, C. G. Overberger, G. Menges, and J. I. Kroschwitz, Eds., Wiley, New York, 1988, Vol. 13, pp. 1–30.
4. A. S. Hay, P. Shenian, A. C. Gowan, P. F. Erhardt, W. R. Haaf, and J. E. Theberge, in *Encyclopedia of Polymer Science and Technology,* 1st ed., H. F. Mark, N. G. Gaylord, and N. M. Bikales, Eds., Interscience, New York, 1969, Vol. 10, pp. 92–111.
5. D. M. White, in *Comprehensive Polymer Science,* Vol. 5: *Step Polymerisation,* G. C. Eastmond, A. Ledwith, S. Russo, and P. Sigwalt, Eds., Pergamon, Oxford, 1989, pp. 473–481.
6. A. S. Hay, H. S. Blanchard, G. F. Endres, and J. W. Eustance, *J. Am. Chem. Soc.,* **81,** 6335 (1959).
7. A. S. Hay, *J. Polym. Sci.,* **58,** 581 (1962).
8. G. F. Endres and J. Kwiatek, *J. Polym. Sci.,* **58,** 593 (1962).
9. G. F. Endres, A. S. Hay, and J. W. Eustance, *J. Org. Chem.,* **28,** 1300 (1963).
10. H. Finkbeiner, A. S. Hay, H. S. Blanchard, and G. F. Endres, *J. Org. Chem.,* **31,** 549 (1966).
11. E. Tsuchida, M. Kaneko, and H. Nishide, *Makromol. Chem.,* **151,** 221 (1972).
12. D. P. Mobley, *J. Polym. Sci. Polym. Chem. Ed.,* **22,** 3203 (1984).
13. S. K. Gupta and A. Kumar, *Reaction Engineering of Step Growth Polymerisation,* Plenum, New York, 1987.
14. A. Kumar and S. K. Gupta, *J. Macromol. Sci. Rev. Macromol. Chem. Phys. C,* **26,** 183 (1986).
15. M. Box, *Comput. J.,* **8,** 42 (1965).
16. M. Sau and S. K. Gupta, *Polymer,* **34,** 4417 (1993).
17. R. E. Treybal, *Mass Transfer Operations,* 3rd ed., McGraw-Hill, New York, 1980, pp. 153–157.
18. R. H. Perry, D. W. Green, and J. O. Maloney, *Perry's Chemical Engineers' Handbook,* 6th ed., McGraw-Hill, New York, 1984.
19. W. L. McCabe, J. C. Smith, and P. Harriott, *Unit Operations of Chemical Engineering,* 4th ed., McGraw-Hill, New York, 1985, pp. 142–143.
20. R. C. Reid, J. M. Prausnitz, and B. E. Poling, *The Properties of Gases and Liquids,* 4th ed., McGraw-Hill, New York, 1988.
21. R. C. Weast, Ed., *Handbook of Chemistry and Physics,* 48th ed., CRC Press, Boca Raton, FL, 1967, pp. F32, F40, F43.
22. D. J. Williams and R. Kreilick, *J. Am. Chem. Soc.,* **89,** 3408 (1967).
23. S. T. Kuberkar and S. K. Gupta, *J. Polym. Eng.,* to appear.
24. S. K. Gupta, *Numerical Methods for Engineers,* Wiley Eastern/New Age, New Delhi, 1995.

Received April 9, 1995
Accepted May 19, 1995